Simultaneous DC-Link and Stator Current Ripple Reduction With Interleaved Carriers in Multiphase Controlled Integrated Modular Motor Drives

Lynn Verkroost ©, *Student Member, IEEE*, Jordi Van Damme ©, *Student Member, IEEE*,
Dimitar V. Bozalakov ©, *Member, IEEE*, Frederik De Belie ©, *Member, IEEE*,
Peter Sergeant ©, *Senior Member, IEEE*, and Hendrik Vansompel ©

Abstract—**To meet the demand for increasingly high power density in electric drives, the concept of a so-called integrated modular motor drive has emerged. The machine is composed of multiple identical modules, which receive individual control signals for multiphase control, to reduce unwanted stator current harmonics. Each module is equipped with its own power electronic converter, which is integrated in the machine housing. This integration imposes strict constraints on the dc-link capacitor design. To reduce the dc-link current ripple, and hence relax the design constraints on the dc-link capacitor, without compromising the possibility to eliminate unwanted stator current harmonics by means of multiphase control, a new interleaving strategy is proposed in this article. The n modules of the machine are split into p subgroups of m modules for interleaving, while the n-phase control is preserved. An analytical model, simulations and experimental results are provided for a 4 kW test setup, confirming that multiphase control can be combined with interleaving. As a result, both the stator current harmonic distortion and the dc-link current ripple can be reduced simultaneously.**

Index Terms—**DC-link capacitor, integrated modular motor drive (IMMD), interleaving, multiphase.**

I. INTRODUCTION

THE HIGH energy efficiency, high power density, and high operating temperatures of emerging power electronic technologies make so-called integrated modular motor drives (IMMDs) a viable possibility [1], [2]: the power electronic converters are integrated in the machine housing and the machine is discretized into n separate modules. Each module consists of a stator segment with a concentrated winding, fed by a dedicated converter and controller. The stator of an axial flux permanent magnet synchronous machine (AFPMSM) with yokeless and segmented armature (YASA) topology is composed of n separate stator core elements [3]. Therefore, its design is inherently suited to be adapted to an IMMD, as is illustrated in Fig. 1. Due to its high efficiency, low weight and compactness, and the resulting high power density, an AFPMSM with YASA topology can be used in transport, energy, and industrial applications [3]–[5].

Their modular design makes IMMDs benefit from economies of scale. The partitioning of the power over the separate modules also results in lower individual component ratings. Besides, an increased power density of the motor-drive combination can be obtained due to the volume decrease as a result of the shared housing.
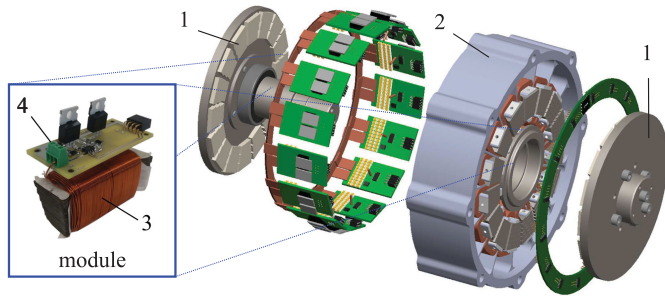
Another advantage of an IMMD, is the feature that the current in each of the n stator modules can be controlled separately. The additional degrees of freedom in such a multiphase control can be utilized for multiple purposes [6]–[8]. A variety of transformations has been proposed to decompose the n-dimensional space into decoupled, orthogonal subspaces that can be controlled independently [9], [10]. These subspaces allow to control not only the fundamental component of the stator current but also its harmonic content. Stator current harmonics which do not contribute to the torque production—but cause stator current ripple and additional losses—can hence be reduced. Karttunen *et al.* [11] use a disturbance observer for this purpose, while Jones *et al.* [12] and Yepes *et al.* [13] use, respectively, additional proportional-integral (PI) and resonant controllers. Another possibility is to enhance the torque production by stator current harmonic injection [14], [15]. The additional degrees of

Fig. 1. Concept of an IMMD: the AFPMSM consists of (1) two rotor discs with permanent magnets, (2) a motor housing and heatsink, and n modules. A module consists of (3) a stator core element with a concentrated winding and (4) its dedicated power electronic converter, which is integrated in the machine housing.

Fig. 2. Interleaving strategies for $n = 6$ modules, divided into $p = 2$ subgroups of $m = 3$ modules. (a) Traditional interleaving strategy: each subgroup gets a dedicated carrier waveform, but the same m-phase reference. (b) Proposed interleaving strategy: each subgroup gets a dedicated carrier waveform, and the references remain n-phase.

freedom under multiphase control also prove useful for fault-tolerant control [7], [8]. They can be deployed, for instance, to improve the current quality [16], to contribute to the torque production [17], or to deliver maximum available ripple-free torque with minimum copper losses [18].

The main disadvantage of IMMDs, on the other hand, is the exposure of the power electronic components to the high temperatures, vibrations, and electromagnetic fields in the machine housing. Jahns and Dai [19] indicate that one of the key technical challenges for full adoption of IMMDs is the reliability of the power electronics (PEs): the lifetime of the PEs must match or exceed the lifetime of the electric machine. Besides, the integration severely limits the permitted volume of the PEs. To tackle these two challenges, stringent requirements are imposed on the design of the dc-link capacitor, as 30% of the failures in PE systems is due to capacitor failure [20], and dc-link capacitors and other passive components occupy up to 30% of the total volume of the PEs [21]. The lifetime and size of the dc-link capacitor are strongly related to the dc-link current ripple. High dc-link current ripple increases the core temperature of an electrolytic dc-link capacitor and hence accelerates its degradation process and the corresponding capacitance drop [22]–[24]. The reduction of the dc-link current ripple is hence key to address the challenges in the PE design of IMMDs. Nevertheless, other dc-link capacitor design considerations, such as dc-link voltage ripple reduction or energy storage capacity, should be taken into account as well [25]. Although an elaborate study on the effect of dc-link voltage ripple constraints on the dc-link capacitor design falls outside the scope of this article, it is interesting to note that the peak-to-peak dc-link voltage ripple amplitude is proportional to the dc-link current ripple [22].

Interleaving of the carrier waveforms for pulsewidth modulation (PWM) is a solution to obtain a dc-link current ripple reduction in a two-level voltage source inverter (2L-VSI). A similar principle can be applied, for instance, to reduce the input current ripple of a dc/dc converter [26], [27] or boost converter [28]–[30], to decrease the output current ripple of a three-phase buck converter [31], or to reduce the torque ripple in sectored multi three-phase machines [32]. To interleave with an n-phase 2L-VSI, the n phases are split into p subgroups of
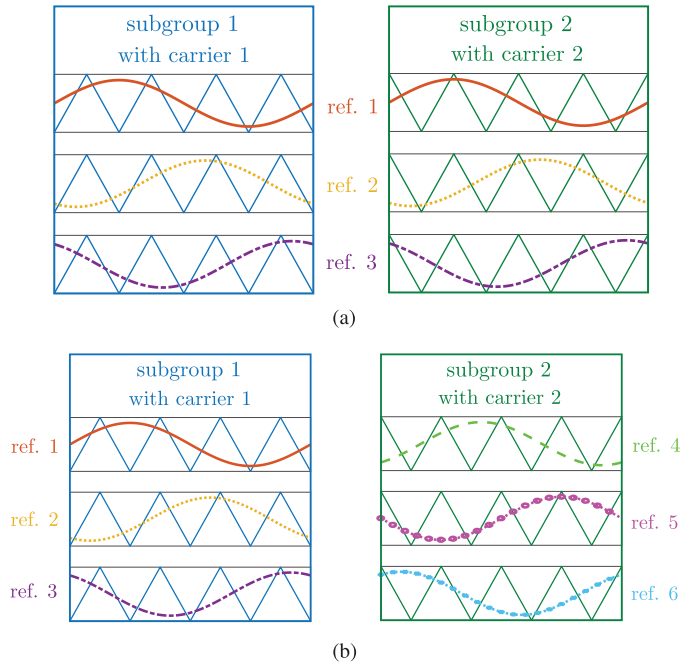
m phases ($n = p \cdot m$). Each group has a dedicated carrier wave, which is shifted with respect to the carrier waves of the other subgroups. In [23], it is experimentally verified that this interleaving technique allows to reduce both the dc-link capacitance and the dc-link capacitor volume of a 55 kW inverter prototype by 60%, while still reducing the capacitor ripple current by 55%–75% as well. However—just as in the other papers where this interleaving technique is applied to the inverter of a segmented multiphase machine [33], [34] or an IMMD [35]–[37]—this interleaving technique is accompanied by a downgrade from an n-phase control to an m-phase control. According to this traditional interleaving strategy, which is illustrated in Fig. 2(a), each subgroup gets a dedicated carrier waveform, but the same m-phase reference as the other subgroups. As a result, the traditional interleaving strategy properly addresses the challenges concerning the PE design of an IMMD on the one hand, but impedes the benefits of multiphase control on the other hand by reducing the available degrees of freedom for the stator current control.

Therefore, the aim and novel contribution of this article is to combine the advantageous effects of multiphase control and interleaving. The n phases are divided into p subgroups for interleaving, but the n-phase control is preserved and each phase receives a different voltage reference, as is illustrated in Fig. 2(b). It is chosen to use the additional degrees of freedom of the multiphase control to reduce the stator current ripple and its harmonic distortion. The reduction in dc-link current ripple with this new interleaving strategy (which is a combination of multiphase control and interleaving) is compared to the

Table	0	0	1	2	3	4
	-6	-5	-4	-3	-2	-1
H-vector	[0	0	1	-3	3	-1]

Table	0	1	2	3	4	5	6
	-7	-6	-5	-4	-3	-2	-1
H-vector	[0	1	-5	3	-3	5	-1]

reduction obtained with traditional interleaving (in which interleaving comes at the expense of a downgrade from n-phase to m-phase control). The difference in stator current ripple and harmonic distortion is investigated as well. Simulation and experimental results are provided for a 4 kW AFPMSM with 15 modules. Contrary to [38], the method is generalized for other topologies, more technical information about the control- and interleaving strategies is provided, an analytical study is conducted and a comprehensive experimental validation is included.

II. MACHINE MODEL DESCRIPTION

The model of the surface-mounted AFPMSM is described in multiple orthogonal dq-reference frames, rotating in synchronism with the current harmonics that need to be controlled. For this purpose, the generalized Clarke and Park transformation matrix $\mathbf{T} = \mathbf{PZF}$ is used, which is elaborated in [9]. $\mathbf{F}$, $\mathbf{Z}$, and $\mathbf{P}$ are three $m \times m$ matrices, with m the amount of phases. The elements of the Fourier transformation matrix $\mathbf{F}$ are defined as

$$f_{ik} = \frac{1}{m} e^{j \frac{2\pi}{m}(i-1)(k-1)}, \quad i, k \in \{1, \ldots, m\}, \quad j^2 = -1. \tag{1}$$

For the inverse matrix $\mathbf{F}^{-1}$ applies

$$(f^{-1})_{ik} = e^{-j \frac{2\pi}{m}(i-1)(k-1)}. \tag{2}$$

The diagonal rotation matrix $\mathbf{Z}$ has the following elements:

$$z_{11} = 1, \quad z_{ik} = 0, \quad z_{ii} = e^{j h_i N_{\mathrm{P}}(\theta - \theta_{0,i})} \tag{3}$$

with θ the mechanical angle, N_{P} the number of pole pairs, h_i the harmonic order, and $\theta_{0,i}$ the phase offset of that particular harmonic. The considered harmonics h_i are elements of a vector $\mathbf{H}$, with $h_1 = 0$ and $h_i = -h_{m-i+2}$ ($i = 2, .., \lceil m/2 \rceil$) for odd m, and $h_1 = h_2 = 0$ and $h_i = -h_{m-i+3}$ ($i = 3, \ldots, m/2 + 1$) for even m. To construct this **H**-vector, the procedure described in [9] is followed. First, the harmonics that need to be regulated are selected. Second, a table is constructed to determine the sequence of these harmonics in the **H**-vector. The first line of this table is a sequence 0, 1, 2, ..., $m - 1$ for odd m, and a sequence 0, 0, 1, 2, ..., $m - 2$ for even m, written from left to right. The second line is a sequence $-1, -2, \ldots, -m$ for both odd and even m, written from right to left. Finally, the correct sequence of the coefficients matching the harmonics that need to be regulated can be read from the table, as is illustrated in Table I and II for a 6- and 7-phase machine, respectively.

The elements of the complex permutation matrix $\mathbf{P}$ are expressed as follows in [9]:

$$p_{ik} = \begin{cases} 1 \Leftrightarrow i = k = 1 \\ 1 \Leftrightarrow ((i = k) \vee (i = m + 2 - k)) \wedge (m + 2 - i > i) \\ j(1 - 2 \cdot \mathrm{mod}(i, 2)) \Leftrightarrow (i = k) \wedge (m + 2 - i \leq i) \\ -j(1 - 2 \cdot \mathrm{mod}(i, 2)) \Leftrightarrow (i = m + 2 - k) \wedge (k \leq i). \end{cases} \tag{4}$$

The inverse matrix $\mathbf{P}^{-1}$ has the following elements:

$$(p^{-1})_{ik} = \begin{cases} 1 \Leftrightarrow i = k = 1 \\ \frac{1}{2} \Leftrightarrow ((i = k) \vee (i = m + 2 - k)) \\ \quad \wedge (m + 2 - k > k) \\ -\frac{1}{2} j(1 - 2 \cdot \mathrm{mod}(k, 2)) \Leftrightarrow (i = k) \\ \quad \wedge (m + 2 - k \leq k) \\ \frac{1}{2} j(1 - 2 \cdot \mathrm{mod}(k, 2)) \Leftrightarrow (i = m + 2 - k) \\ \quad \wedge (i \leq k) \end{cases} . \tag{5}$$

The advantage of this generalized transformation is that it can be used for an arbitrary number of phases m.

After applying the Clarke and Park transformation, the model of the AFPMSM can be written in the following form:

$$v_{\mathrm{dh}} = R_s i_{\mathrm{dh}} + L_h \frac{d i_{\mathrm{dh}}}{dt} - N_{\mathrm{P}} h \Omega L_h i_{\mathrm{qh}} \tag{6}$$

$$v_{\mathrm{qh}} = R_s i_{\mathrm{qh}} + L_h \frac{d i_{\mathrm{qh}}}{dt} + N_{\mathrm{P}} h \Omega L_h (i_{\mathrm{dh}} + i_{\mathrm{PM},h}). \tag{7}$$

R_{s} (Ω) represents the stator winding resistance per stator module; N_{p} the number of pole pairs; h the harmonic order; Ω (rad/s) the mechanical speed. The permanent magnets are represented by i_{PM}, which is a constant equivalent current along the d-axis, resulting in the same flux level as generated by the permanent magnets. The stator inductances L for the d- and q-axis are approximately the same, because the considered AFPMSM has surface-mounted permanent magnets. The inductances in the dq-reference frame are derived from the experimentally determined self inductances $L_{x,x}$ and mutual inductances $L_{x,y}$ ($x, y \in \{1, \ldots, m\}, x \neq y$)

$$\mathbf{L_{dq}} = \mathbf{T L_{abc} T}^{-1} \tag{8}$$

with $\mathbf{L_{dq}} = \mathrm{diag}([L_{|h_1|}, L_{|h_2|}, \ldots, L_{|h_m|}])$ and

$$\mathbf{L_{abc}} = \begin{bmatrix} L_{1,1} & L_{1,2} & \cdots & L_{1,m-1} & L_{1,m} \\ L_{2,1} & L_{2,2} & \cdots & L_{2,m-1} & L_{2,m} \\ \vdots & \vdots & \ddots & \vdots & \vdots \\ L_{m-1,1} & L_{m-1,2} & \cdots & L_{m-1,m-1} & L_{m-1,m} \\ L_{m,1} & L_{m,2} & \cdots & L_{m,m-1} & L_{m,m} \end{bmatrix} .$$

To obtain experimental values for $L_{x,y}$, only winding y is supplied with current by means of a 50 Hz ac-excitation, and all other windings are open-circuited. The induced voltage is then measured in stator winding x.

The stator voltages v and currents i in the dq-reference frame of the harmonic h are obtained by applying the Clarke and Park
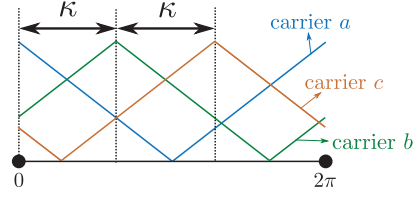
(a)

(b)

(c)
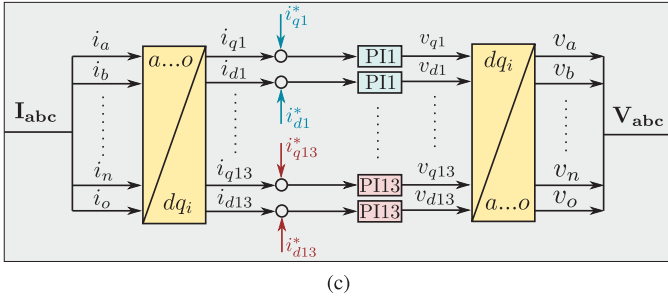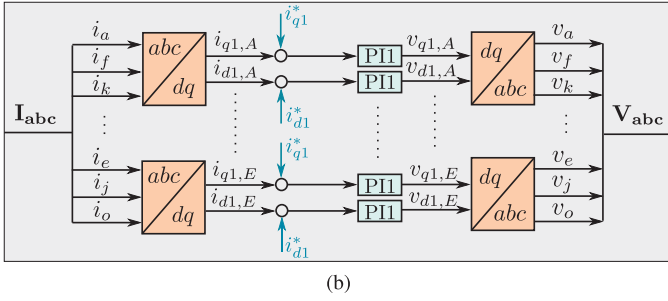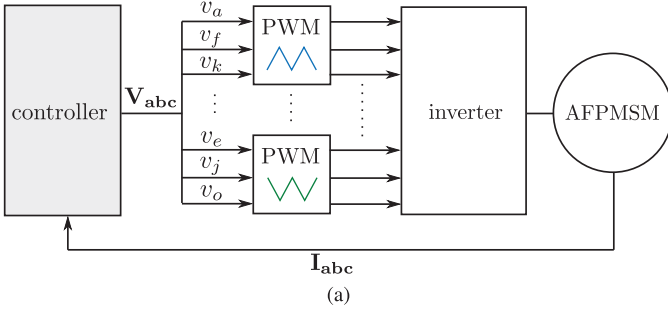
Fig. 3. (a) General control structure for $[p, m] = [5, 3]$ with (b) five times 3-phase PI control under the traditional strategy, which can only control the fundamental stator current component, or (c) 15-phase PI control under the proposed strategy, which can control seven harmonic stator current components. In (a) it is shown that the 15 phases are split into 5 subgroups of 3 phases for reduction of the dc-link current ripple by means of interleaving for both (b) and (c).

Fig. 4. Definition of the interleaving angle κ between the carrier waves.

harmonics is controlled by two PI controllers: one to control i_{qh} and one to control i_{dh}.

As one of the goals of this article is to compare the stator current ripple obtained with the different strategies; an objective quantification of this ripple is defined by means of its root mean square (rms) value

$$\text{rms}(\Delta i_{q1}) = \sqrt{\frac{1}{s} \sum_{k=1}^{s} \left(i_{q1}(k) - \bar{i}_{q1} \right)^2}. \quad (10)$$

$\bar{i}_{q1}$ is the average value of i_{q1} over the considered s samples. The weighted total harmonic distortion (WTHD) can provide an objective quantification of the stator current ripple as well. This parameter is defined as follows:

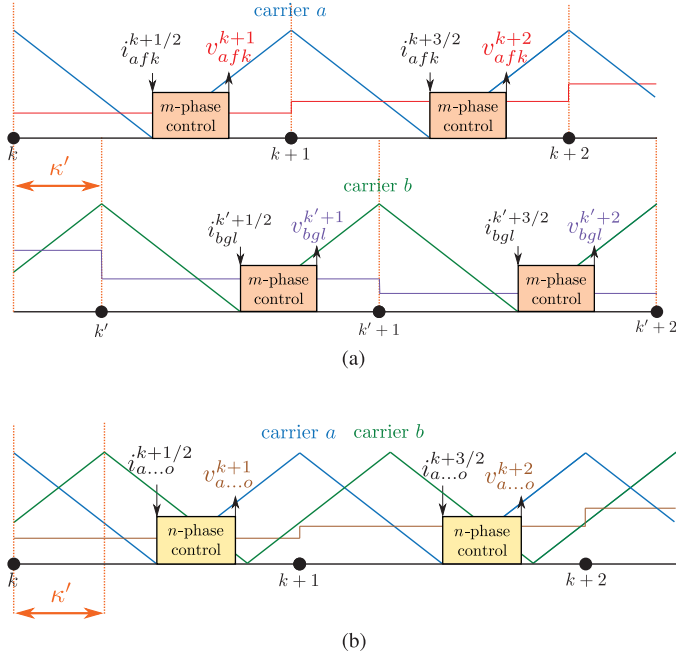$$\text{WTHD}(i_a) = \frac{1}{I_{a1}} \sum_{h \neq 1} \left(\frac{I_{ah}}{h} \right)^2 \quad (11)$$

with I_{ah} the modulus of the hth harmonic in i_a.

It is expected that the n-phase control of the proposed interleaving strategy results in lower $\text{rms}(\Delta i_{q1})$ and lower $\text{WTHD}(i_a)$, which will be verified in the case study of Section VI.

IV. INTERLEAVING STRATEGIES

In this section, interleaving will be introduced in order to reduce the dc-link current ripple. Each subgroup—consisting of m modules connected in star—gets its own carrier wave to generate the PWM signals that drive the n-phase 2L-VSI. These carrier waves are shifted with respect to each other with an interleaving angle κ, which is defined in Fig. 4. Due to the shift between the carrier waves, there is also a shift between the phase voltage pulses of the subgroups, which in turn causes a shift between the phase current ripples. As the dc-link current contains the sum of all the phase currents, the dc-link current ripple will be lower as compared to the situation without interleaving, in which all phase current ripples are in phase.

Two interleaving strategies will be investigated in this article. Their working principle is illustrated in Fig. 5. The first strategy, depicted in Fig. 5(a), corresponds to traditional interleaving. When the n modules are divided into p subgroups of m modules, each subgroup gets its own m-phase controller and its own time line, shifted with a time step $\kappa' = \kappa/(2\pi f_u)$. As the m-phase control only needs information about the current in its own m modules, the current and rotor position measurements do not need to be performed simultaneously for the p subgroups. As a result, the current and rotor position measurements are always performed in the middle of the period of the carrier wave corresponding to the subgroup under consideration, i.e., at

transformations to the phase voltages and currents

$$\mathbf{V_{dq}} = \mathbf{T V_{abc}}, \qquad \mathbf{I_{dq}} = \mathbf{T I_{abc}}. \quad (9)$$

III. PI CONTROL STRATEGIES

The n modules of an IMMD can be divided into p subgroups of m modules. The modules belonging to the same subgroup are connected in a neutral point, giving p m-phase stars. For traditional interleaving, this division implies that the phase current control downgrades from an n-phase control to an m-phase control, which can eliminate less harmonic orders. The proposed interleaving strategy, which will be elaborated in Section IV, aims to preserve the n-phase control. The control structure depicted in Fig. 3 for $[p, m]$ equal to $[5, 3]$ is used to study the difference between the different control strategies: p independent m-phase controllers as in Fig. 3(b), or one n-phase controller as in Fig. 3(c). The phase currents of each subgroup are transformed by means of the m- or n-phase Clarke and Park transformation, respectively, explained in Section II. Each of the

Fig. 5. Interleaving strategies. (a) Traditional interleaving strategy: the carriers, the current measurements, the m-phase PI control and the voltage references are all shifted per group. (b) Proposed interleaving strategy: only the carriers are shifted. The current measurements for the n modules, the n-phase PI control and the resulting n-phase voltage reference remain simultaneous.

instant $k + 1/2$ for the first, nonshifted subgroup with carrier a and at instant $k' + 1/2$ for the second, shifted subgroup with carrier b. The m-phase PI controllers calculate the m-phase voltages that need to be applied during the next time step, respectively, $k + 1 \to k + 2$ and $k' + 1 \to k' + 2$ for the two illustrated subgroups. As a result, the voltage reference for a subgroup always changes at the beginning of a new period of the carrier wave of that subgroup.

The second interleaving strategy is presented in Fig. 5(b) and corresponds to the new, proposed interleaving strategy. In this strategy, the n modules are split in p subgroups of m modules for interleaving, but the n-phase control is preserved. This implies that the n-phase controller needs information about all n phase currents to apply the n-phase transformation described in Section II, and not only about the m phase currents belonging to one subgroup. Therefore, all n phase currents are measured in the middle of carrier wave a of the first, nonshifted subgroup, after which the n-phase controller determines the n-phase voltage that will be applied during the next time interval $k + 1 \to k + 2$. Contrary to the traditional interleaving strategy, now only the carrier waveforms are shifted with respect to each other. As a result, the voltage reference for a subgroup does not necessarily change at the beginning of a new period of the corresponding carrier wave, as is shown for carrier b in Fig. 5(b).

V. ANALYTICAL MODEL OF THE DC-LINK CURRENT UNDER INTERLEAVING

In this section, an analytical model for the dc-link current ripple is provided. Each stator winding of the IMMD is fed by
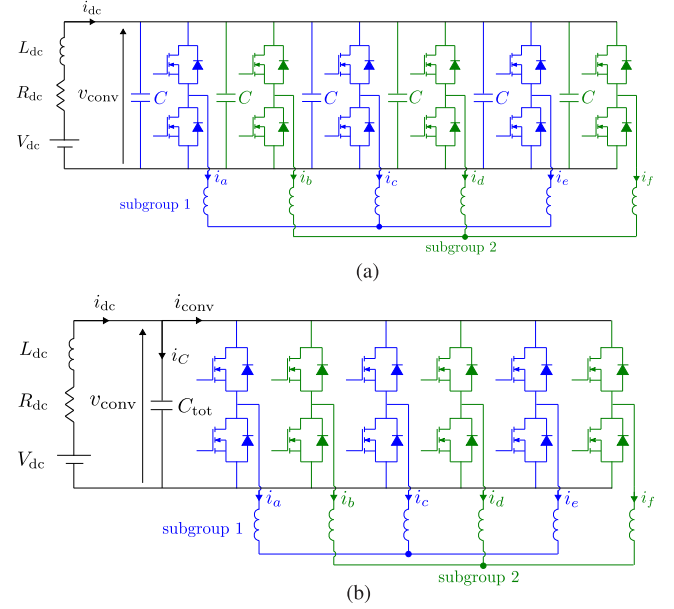
Fig. 6. Schematic overview of the modules with their dedicated converters for $[p, m] = [2, 3]$. Parasitic inductances between the modules are neglected. (a) Original circuit. (b) Simplified circuit.

a dedicated converter leg, with a dedicated dc-link capacitor C, as is illustrated in Fig. 6(a). When parasitic inductances between the modules are neglected, the circuit can be simplified into Fig. 6(b) by combining all the capacitors into one single capacitor C_{tot}. The dynamics of the converter can be expressed as

$$V_{\text{dc}} = R_{\text{dc}} i_{\text{dc}} + L_{\text{dc}} \frac{d i_{\text{dc}}}{dt} + v_{\text{conv}} \tag{12}$$

$$C_{\text{tot}} \frac{d v_{\text{conv}}}{dt} = i_{\text{dc}} - i_{\text{conv}} \tag{13}$$

with V_{dc}, i_{dc}, R_{dc}, and L_{dc}, respectively, the dc-link voltage, -current, -resistance, and -inductance. v_{conv} and i_{conv} are, respectively, the input voltage and -current of the converter itself, with $i_{\text{conv}} = \sum_x s_x i_x$. s_x and i_x are, respectively, the binary switching function and the phase current of phase x. In case of ideal switches, s_x equals 1 if the upper switch of phase x is ON, and the lower switch is OFF. s_x equals 0 if the lower switch of phase x is ON, and the upper switch is OFF.

The dc-link current i_{dc} at frequency ω can hence be expressed as

$$I_{\text{dc}}(\omega) = \frac{\sum_x (S_x \otimes I_x)(\omega)}{1 - \omega^2 L_{\text{dc}} C_{\text{tot}} + j \omega R_{\text{dc}} C_{\text{tot}}}. \tag{14}$$

The symbol $\otimes$ denotes the two-dimensional convolution of the Fourier coefficients. The switching function can be expanded in a double Fourier series [39]–[41]

$$s_x(u, v) = \frac{A_{00}}{2} + \sum_{n=1}^{\infty} [A_{0n} \cos(nv) + B_{0n} \sin(nv)]$$

$$+ \sum_{m=1}^{\infty} \sum_{n=-\infty}^{\infty} [A_{mn} \cos(mu + nv) + B_{mn} \sin(mu + nv)] \tag{15}$$

TABLE III
MACHINE PARAMETERS

Parameter	Symbol	Value
Rated torque (Nm)	T_n	15
Rated speed (rpm)	N_n	2500
Number of pole pairs	N_p	8
Stator winding resistance (mΩ)	R_s	65
Self- and mutual inductances (μH)	$L_{x,x}$	316
	$L_{x,x-1} = L_{x,x+1}$	111
	$L_{x,x-2} = L_{x,x+2}$	15.5
	$L_{x,x-3} = L_{x,x+3}$	9.52
	$L_{x,x-4} = L_{x,x+4}$	8.27
	$L_{x,x-5} = L_{x,x+5}$	6.05
	$L_{x,x-6} = L_{x,x+6}$	6.07
	$L_{x,x-7} = L_{x,x+7}$	5.31
Stator inductance computed by (8) (μH)	L_0	320
	L_1	518
	L_3	357
	L_5	201
	L_7	119
	L_9	144
	L_{11}	275
	L_{13}	437
Equivalent PM current (A)	$i_{PM,1}$	42.5100
	$i_{PM,3}$	3.6870
	$i_{PM,5}$	0.7921
	$i_{PM,7}$	0.1471
	$i_{PM,9}$	0.0906
	$i_{PM,11}$	0.0102
	$i_{PM,13}$	0.0067

where

$$S_{mn} = A_{mn} + jB_{mn}$$
$$= \frac{1}{2\pi^2} \int_{-\pi}^{\pi} \int_{-\frac{\pi}{2}(1+\tilde{v}_x^*(v))+\kappa}^{\frac{\pi}{2}(1+\tilde{v}_x^*(v))+\kappa} e^{j(mu+nv)} du\, dv \qquad (16)$$

with $u = \omega_c t$ and $v = \omega_0 t$. ω_c is the carrier angular frequency, and ω_0 is the fundamental angular frequency of the reference voltage waveform $v_x^*(v)$ of phase x, with $\tilde{v}_x^*(v) = 2v_x^*(v)/V_{dc}$. In case of traditional interleaving, $v_x^*(v)$ originates from an m-phase controller. For the new, proposed interleaving strategy, $v_x^*(v)$ comes from an n-phase controller.

The time-function $i_{dc}(t)$ can be reconstructed from its Fourier coefficients (14) in a similar way as (15), using the relation $\omega = m\omega_c + n\omega_0$.

As the dc-link capacitor (with reactance $1/(\omega_c C_{tot})$) is designed to conduct the high-frequent dc-link current ripple instead of the dc voltage source (with impedance $R_{dc} + j\omega_c L_{dc} > 1/(\omega_c C_{tot})$), the interleaving results in a current ripple reduction in i_C that is even more pronounced than the current ripple reduction in i_{dc}. The stress on the dc-link capacitor can hence effectively be reduced.

VI. CASE STUDY ON A 15-PHASE AFPMSM

To clarify the PI control strategies and interleaving strategies, they will now be implemented on an AFPMSM consisting of 15 modules. Each module is equipped with a dedicated half-bridge inverter leg. The machine parameters are listed in Table III.

For the purpose of the interleaving strategies explained in Section IV, the 15 modules ($\{a, b, c, d, e, f, g, h, i, j, k, l, m, n,$

$o\}$) of the AFPMSM serving as an example in this article, can be connected into the following three topologies:
1) Topology 1: 5 subgroups of 3 modules ($[p,m] = [5,3]$): $\{A = \{a,f,k\}, B = \{b,g,l\}, C = \{c,h,m\}, D = \{d,i,n\}, E = \{e,j,o\}\}$
2) Topology 2: 3 subgroups of 5 modules ($[p,m] = [3,5]$): $\{A' = \{a,d,g,j,m\}, B' = \{b,e,h,k,n\}, C' = \{c,f,i,l,o\}\}$
3) Topology 3: 1 group of 15 modules ($[p,m] = [1,15]$): $\{A'' = \{a,b,c,d,e,f,g,h,i,j,k,l,m,n,o\}\}$

The modules belonging to the same subgroup are connected in a neutral point, giving, respectively, five 3-phase stars, three 5-phase stars, or one 15-phase star.

A. Stator Current Ripple Reduction

For a 15-phase control, seven harmonics can be considered according to Section II: $h \in \{1, 3, 5, 7, 9, 11, 13\}$, and hence $\mathbf{H} = [0, 1, -13, 3, -11, 5, -9, 7, -7, 9, -5, 11, -3, 13, -1]$ and $\mathbf{L_{dq}} = \text{diag}([L_0, L_1, L_{13}, L_3, L_{11}, L_5, L_9, L_7, L_7, L_9, L_5, L_{11}, L_3, L_{13}, L_1])$. For three subgroups with 5-phase control, only the first and third harmonic can be regulated. The $\mathbf{H}$-vector diminishes to $\mathbf{H} = [0, 1, -3, 3, -1]$ and $\mathbf{L_{dq}}$ to $\text{diag}([L_0, L_1, L_3, L_3, L_1])$. For five subgroups with 3-phase control, only the fundamental ($h = 1$) can be considered, with $\mathbf{H} = [0, 1, -1]$ and $\mathbf{L_{dq}} = \text{diag}([L_0, L_1, L_1])$. The reference value i_{q1}^* is proportional to the torque in this case, whereas maximum torque per ampere is obtained by setting i_{d1}^* equal to zero. For the other topologies, it is chosen to keep i_{q1}^* proportional to the torque, and to control the other i_{qh} and i_{dh} to zero. In other words, torque enhancement by injecting low-order current harmonics is not studied here.

Fig. 7 shows the simulation results for i_{q1}^* equal to 7 A, a mechanical speed N of 700 r/min, a dc-link voltage V_{dc} of 48 V, and an update frequency f_u of the controller of 50 kHz. As can be seen in Fig. 7(a), the 15-phase control of the proposed interleaving strategy indeed leads to a lower q-current ripple than the 3- and 5- phase control of the conventional interleaving strategy, for both $[p,m] = [5,3]$ and $[3,5]$. The stator current ripple is almost not affected by the interleaving angle κ. On average, $\text{rms}(\Delta i_{q1})$ is equal to 0.4105 A for 3-phase control ($[p,m] = [5,3]$), 0.0735 A for 5-phase control ($[p,m] = [3,5]$), and 0.0137 A for 15-phase control ($[p,m] = [5,3]$ or $[p,m] = [3,5]$). However, the difference between the 5- and 15-phase control is modest, due to the fact that the seventh harmonic is not strongly present. Similar conclusions can be drawn from the WTHD of the phase current i_a, which is presented in Fig. 7(b). The average $\text{WTHD}(i_a)$ amounts to 0.0133 A for 3-phase control, 0.0037 A for 5-phase control, and 0.0035 A for 15-phase control.

It must be noted, however, that for a traditional 3-phase current controller $\text{rms}(\Delta i_{q1})$ amounts to only 0.0824 A, and $\text{WTHD}(i_a)$ to only 0.0018 A for $V_{dc} = 240$ V. With traditional 3-phase controller is meant in this context that five modules are connected in series to constitute one phase, and that the resulting three phases are fed by means of a traditional 3-phase 2L-VSI. The fact that this traditional 3-phase control results in less stator
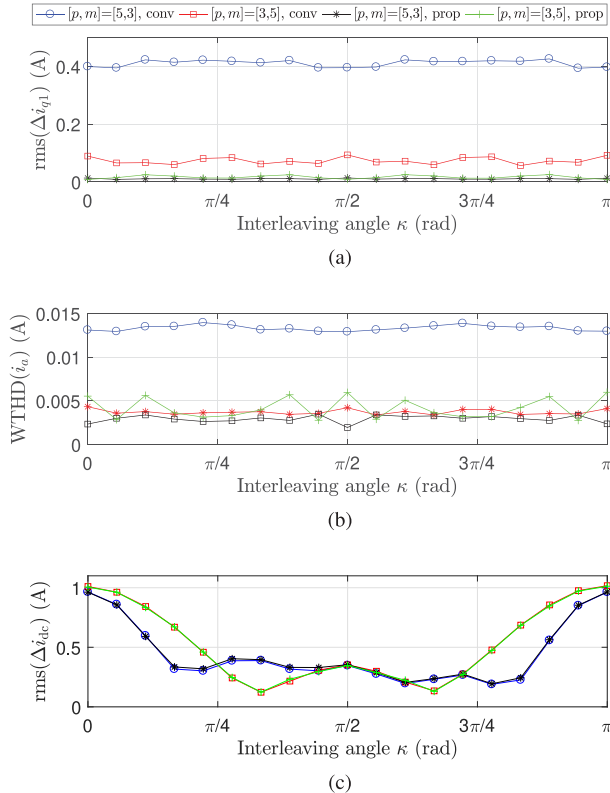
(a)

(b)

(c)

Fig. 7.   Simulation results for the conventional and proposed interleaving strategy ($i_{q1}^* = 7$ A, $N = 700$ r/min).

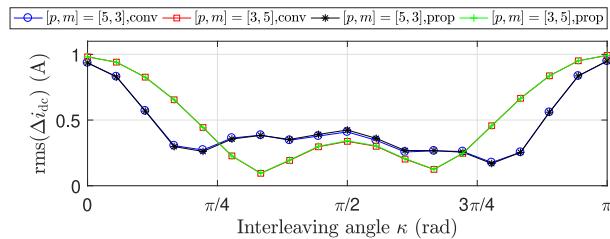Fig. 8.   Analytical results for the conventional and proposed interleaving strategy ($i_{q1}^* = 7$ A, $N = 700$ r/min).

current ripple than the five times 3-phase control in which each module constitutes a phase on its own, can be explained by the difference in higher order harmonic winding factor. The higher order harmonic winding factor of the arrangement with one phase of the 3-phase controller consisting of five modules in series is lower than for the arrangement in which one module constitutes one phase.

B. DC-Link Current Ripple Reduction

The analytical results of Fig. 8—which are obtained with the analytical model introduced in Section V—show how the current ripple in the dc-link varies with $\kappa \in [0, \pi]$ for both $[p, m] = [5, 3]$ and $[p, m] = [3, 5]$. Symmetrical results are obtained for $\kappa \in [\pi, 2\pi]$. The parameter rms(Δi_{dc}) is computed in the same way as rms(Δi_{q1}), i.e., according to (10). Under the proposed
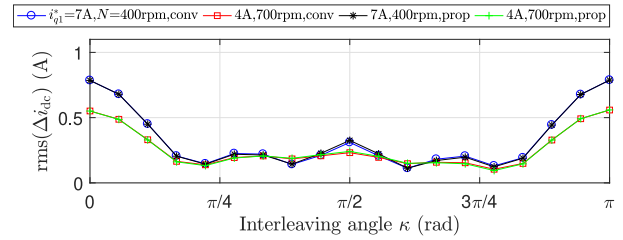

Fig. 9.   Analytical results for the conventional and proposed interleaving strategy under different operating points for the topology $[p, m] = [5, 3]$.

interleaving strategy, the reference voltage waveform v_x^* contains harmonics $h \in \{1, 3, 5, 7, 9, 11, 13\}$ in order to obtain WTHD(i_a) = 0 A for both $[p, m] = [5, 3]$ and $[p, m] = [3, 5]$. For $[p, m] = [5, 3]$, $v_x^*(v)$ only contains a fundamental component under conventional interleaving, resulting in a WTHD(i_a) of 0.0095 A. For $[p, m] = [3, 5]$ under conventional interleaving, v_x^* also includes a third harmonic component, which decreases WTHD(i_a) to 0.0018 A. The analytical results for rms(Δi_{dc}) are almost identical to the simulation results shown in Fig. 7(c). Both the analytical and simulated results are obtained for a dc-link capacitance of 1 mF per module, resulting in a total dc-link capacitance of 15 mF. A dc-link inductance is not considered; the dc-link resistance equals 1.5 mΩ. It can be concluded that both interleaving strategies result in a similar dc-link current ripple. For $[p, m] = [5, 3]$ the lowest dc-link current ripple is obtained for $\kappa = 4\pi/18$ or $14\pi/18$ rad. For these optimal interleaving angles, rms(Δi_{dc}) equals 0.1821 A, which is a reduction of more than 80% compared to the 0.9497 A without interleaving. For $[p, m] = [3, 5]$, the minimal dc-link current ripple of 0.1287 A is obtained for $\kappa = 6\pi/18$ or $12\pi/18$ rad, which is a reduction of 87% compared to the dc-link current ripple for $\kappa = 0$ rad. However, $[p, m] = [5, 3]$ is the preferred topology, as the decrease in rms(Δi_{dc}) is less dependent on κ: for $\kappa \in [3\pi/18, 15\pi/18]$ the waveform of rms(Δi_{dc}) in function of κ remains quite flat. Fig. 9 shows that similar conclusions hold under different operating points (i.e., different i_{q1}^* and N) as well.

VII. EXPERIMENTAL VALIDATION

To validate the features of the conventional and the proposed interleaving strategy, both algorithms are implemented on the FPGA of a dSPACE MicroLabBox. The experiments are conducted on the 4 kW AFPMSM shown in Fig. 10, consisting of 15 modules and with the specifications of Table III. The stator phase current measurements are obtained from the current transducers which provide feedback to the controllers at 50 kHz, and are processed in the MicroLabBox. The dc-link current is measured at 100 MHz with a Tektronix TCPA300. The experiments are conducted under $N = 700$ r/min, $i_{q1}^* = 7$ A, $f_u = 50$ kHz, $V_{dc} = 48$ V, and a dead time of 1 μs, unless stated otherwise. Each converter has its own dedicated 1 mF dc-link capacitor, but no dc-link inductor. The experiments are conducted for a $[p, m] = [5, 3]$ topology.
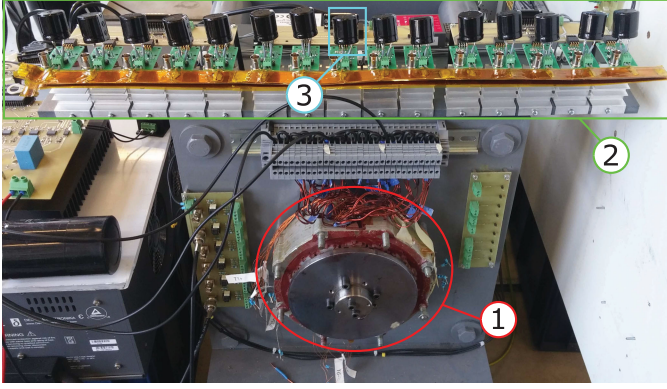
Fig. 10. IMMD test setup comprises (1) an AFPMSM, with (2) a dedicated converter per module, each equipped with (3) an electrolytic dc-link capacitor of 1 mF.
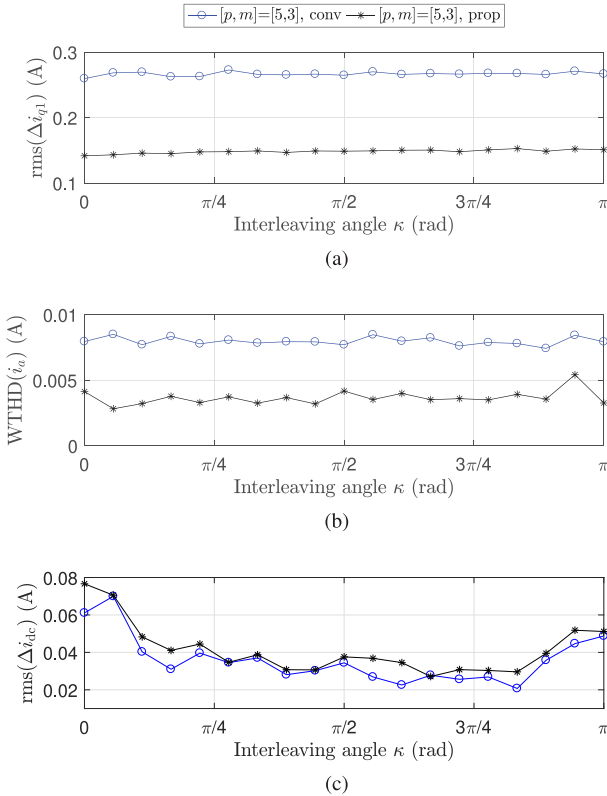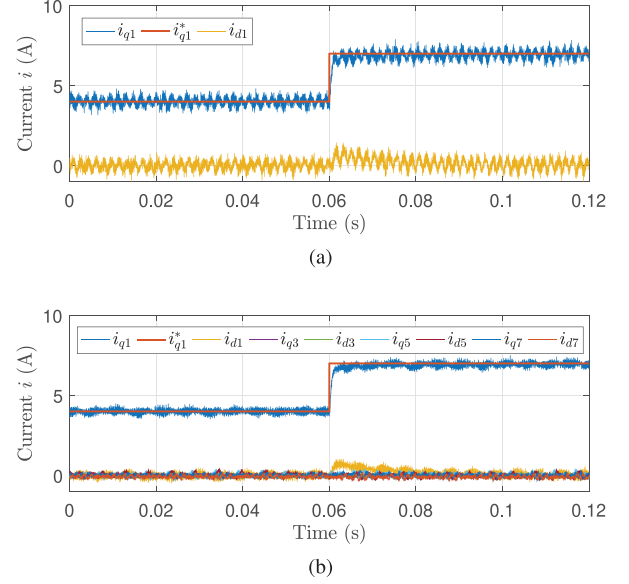

(a)

(b)

Fig. 12. Measured step responses for the conventional and proposed interleaving strategy ($\kappa = 14\pi/18$ rad, $N = 700$ r/min, $[p, m] = [5, 3]$). (a) Conventional interleaving strategy with 3-phase control. (b) Proposed interleaving strategy with 15-phase control.
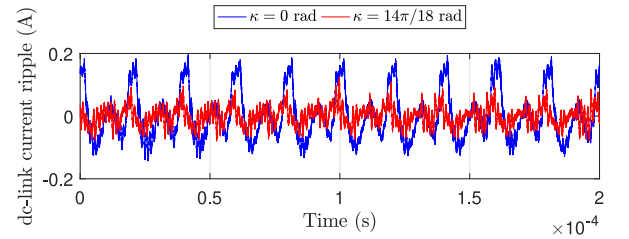

Fig. 13. Measurement of the dc-link current ripple $\Delta i_{\mathrm{dc}} = i_{\mathrm{dc}} - \bar{i}_{\mathrm{dc}}$ ($i_{q1}^{*} = 7$ A, $N = 700$ r/min, $[p, m] = [5, 3]$, proposed strategy, $\bar{i}_{\mathrm{dc}} = 20.1$ A).
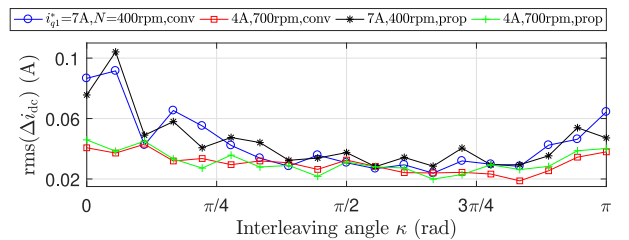

Fig. 14. Experimental results for the conventional and proposed interleaving strategy under different operating points for the topology $[p, m] = [5, 3]$.

(a)

(b)

(c)

Fig. 11. Experimental results for the conventional and proposed interleaving strategy ($i_{q1}^{*} = 7$ A, $N = 700$ r/min, $[p, m] = [5, 3]$).

The performance superiority of the proposed interleaving strategy with regard to the stator current ripple, is confirmed by the results shown in Fig. 11(a). The 15-phase control in the proposed strategy results in a q-current ripple of only 0.1482 A, which is 44% less than for the 3-phase control of the conventional strategy. The difference in q-current ripple can also be observed in the step responses of Fig. 12. The WTHD of the phase current is reduced by more than 50%, as can be seen in Fig. 11(b). The stator current ripple and WTHD are almost not affected by the interleaving angle κ.

Fig. 11(c) shows the dc-link current ripple. It is validated that both interleaving strategies indeed lead to a similar level of dc-link current ripple, and that for $\kappa \in [3\pi/18, 15\pi/18]$ the waveform of rms(Δi_{dc}) in function of κ remains quite flat. For both interleaving strategies, a dc-link current ripple reduction of 58% is obtained in comparison with the situation without interleaving (i.e., $\kappa = 0$). This reduction is clearly visible in the measured dc-link current ripple of Fig. 13 for κ equal to 0 and

$14\pi/18$ rad. The experimental results of Fig. 14 confirm that similar conclusions hold for other operating points as well.

Thus, the experimental results verified that the proposed interleaving strategy combines the advantages of both multiphase control and interleaving: the proposed interleaving strategy results in lower stator current ripple and harmonic distortion than conventional interleaving, while it preserves its ability to lower the dc-link current ripple.

VIII. CONCLUSION

The new interleaving strategy proposed in this article was able to combine the advantageous effects of both traditional interleaving and multiphase control. The proposed interleaving strategy allowed to split the n modules into p subgroups of m modules to reduce the current ripple in the dc-link, while still maintaining an n-phase control instead of an m-phase control to eliminate unwanted stator current harmonics. The performance of the proposed interleaving strategy concerning dc-link current ripple and stator current harmonic distortion was compared to the performance under traditional interleaving by means of simulations for a 4 kW AFPMSM IMMD with 15 modules. Experimental results confirmed that the proposed interleaving strategy results in a similar dc-link current ripple reduction as traditional interleaving, hence effectively relieving the stress on the dc-link capacitor. The fact that the control was not downgraded from a 15-phase control to a 3-phase control under the proposed interleaving strategy, results in a decrease in stator current harmonic distortion compared to the traditional interleaving strategy. The stator current harmonic distortion was not affected by the interleaving.

REFERENCES

[1] A. Shea and T. M. Jahns, "Hardware integration for an integrated modular motor drive including distributed control," in *Proc. IEEE Energy Convers. Congr. Expo.*, Sep. 2014, pp. 4881–4887.

[2] N. R. Brown, T. M. Jahns, and R. D. Lorenz, "Power converter design for an integrated modular motor drive," in *Proc. IEEE Ind. Appl. Annu. Meeting*, Sep. 2007, pp. 1322–1328.

[3] B. Zhang, T. Seidler, R. Dierken, and M. Doppelbauer, "Development of a yokeless and segmented armature axial flux machine," *IEEE Trans. Ind. Electron.*, vol. 63, no. 4, pp. 2062–2071, Apr. 2016.

[4] Y. Park, M. Koo, S. Jang, J. Choi, and D. You, "Performance evaluation of radial- and axial-flux PM wind power generators with mechanical energy storage system," *IEEE Trans. Energy Convers.*, vol. 30, no. 1, pp. 237–245, Mar. 2015.

[5] W. Deng and S. Zuo, "Analytical modeling of the electromagnetic vibration and noise for an external-rotor axial-flux in-wheel motor," *IEEE Trans. Ind. Electron.*, vol. 65, no. 3, pp. 1991–2000, Mar. 2018.

[6] F. Barrero and M. J. Duran, "Recent advances in the design, modeling, and control of multiphase machines - Part I," *IEEE Trans. Ind. Electron.*, vol. 63, no. 1, pp. 449–458, Jan. 2016.

[7] M. J. Duran and F. Barrero, "Recent advances in the design, modeling, and control of multiphase machines - Part II," *IEEE Trans. Ind. Electron.*, vol. 63, no. 1, pp. 459–468, Jan. 2016.

[8] E. Levi, "Multiphase electric machines for variable-speed applications," *IEEE Trans. Ind. Electron.*, vol. 55, no. 5, pp. 1893–1909, May 2008.

[9] J. Figueroa, J. Cros, and P. Viarouge, "Generalized transformations for polyphase phase-modulation motors," *IEEE Trans. Energy Convers.*, vol. 21, no. 2, pp. 332–341, Jun. 2006.

[10] J. Malvar *et al.*, "Graphical diagram for subspace and sequence identification of time harmonics in symmetrical multiphase machines," *IEEE Trans. Ind. Electron.*, vol. 61, no. 1, pp. 29–42, Jan. 2014.

[11] J. Karttunen, S. Kallio, P. Peltoniemi, and P. Silventoinen, "Current harmonic compensation in dual three-phase PMSMs using a disturbance observer," *IEEE Trans. Ind. Electron.*, vol. 63, no. 1, pp. 583–594, Jan. 2016.

[12] M. Jones, S. N. Vukosavic, D. Dujic, and E. Levi, "A synchronous current control scheme for multiphase induction motor drives," *IEEE Trans. Energy Convers.*, vol. 24, no. 4, pp. 860–868, Dec. 2009.

[13] A. G. Yepes, J. Malvar, A. Vidal, O. López, and J. Doval-Gandoy, "Current harmonics compensation based on multiresonant control in synchronous frames for symmetrical n-phase machines," *IEEE Trans. Ind. Electron.*, vol. 62, no. 5, pp. 2708–2720, May. 2015.

[14] L. Zheng, J. E. Fletcher, B. W. Williams, and X. He, "Dual-plane vector control of a five-phase induction machine for an improved flux pattern," *IEEE Trans. Ind. Electron.*, vol. 55, no. 5, pp. 1996–2005, May. 2008.

[15] G. Feng, C. Lai, M. Kelly, and N. C. Kar, "Dual three-phase PMSM torque modeling and maximum torque per peak current control through optimized harmonic current injection," *IEEE Trans. Ind. Electron.*, vol. 66, no. 5, pp. 3356–3368, May. 2019.

[16] H. Lu, J. Li, R. Qu, D. Ye, and Y. Lu, "Fault-tolerant predictive control of six-phase PMSM drives based on pulsewidth modulation," *IEEE Trans. Ind. Electron.*, vol. 66, no. 7, pp. 4992–5003, Jul. 2019.

[17] H. Ryu, J. Kim, and S. Sul, "Synchronous-frame current control of multiphase synchronous motor under asymmetric fault condition due to open phases," *IEEE Trans. Ind. Appl.*, vol. 42, no. 4, pp. 1062–1070, Jul. 2006.

[18] A. Mohammadpour and L. Parsa, "Global fault-tolerant control technique for multiphase permanent-magnet machines," *IEEE Trans. Ind. Appl.*, vol. 51, no. 1, pp. 178–186, Jan. 2015.

[19] T. M. Jahns and H. Dai, "The past, present, and future of power electronics integration technology in motor drives," *CPSS Trans. Power Electron. Appl.*, vol. 2, no. 3, pp. 197–216, Sep. 2017.

[20] H. Wang, M. Liserre, and F. Blaabjerg, "Toward reliable power electronics: Challenges, design tools, and opportunities," *IEEE Ind. Electron. Mag.*, vol. 7, no. 2, pp. 17–26, Jun. 2013.

[21] M. Marz, A. Schletz, B. Eckardt, S. Egelkraut, and H. Rauh, "Power electronics system integration for electric and hybrid vehicles," in *Proc. 6th Int. Conf. Integr. Power Electron. Syst.*, Mar. 2010, pp. 1–10.

[22] M. Vujacic, O. Dordevic, and G. Grandi, "Evaluation of DC-Link voltage switching ripple in multiphase PWM voltage source inverters," *IEEE Trans. Power Electron.*, vol. 35, no. 4, pp. 3478–3490, Apr. 2020.

[23] G. Su and L. Tang, "A segmented traction drive system with a small dc bus capacitor," in *Proc. IEEE Energy Convers. Congr. Expo.*, Sep. 2012, pp. 2847–2853.

[24] M. H. Bierhoff and F. W. Fuchs, "DC-link harmonics of three-phase voltage-source converters influenced by the pulsewidth-modulation strategy - An analysis," *IEEE Trans. Ind. Electron.*, vol. 55, no. 5, pp. 2085–2092, May. 2008.

[25] J. Van Damme, L. Verkroost, H. Vansompel, F. De Belie, and P. Sergeant, "A holistic DC link architecture design method for multiphase integrated modular motor drives," in *Proc. IEEE Int. Electric Mach. Drives Conf.*, IEEE, 2019, pp. 1593–1598.

[26] K. Hu, J. Wang, T. Lin, and C. Liaw, "A switched-reluctance generator with interleaved interface DC-DC converter," *IEEE Trans. Energy Convers.*, vol. 30, no. 1, pp. 273–284, Mar. 2015.

[27] C. Pan, C. Chuang, and C. Chu, "A novel transformerless interleaved high step-down conversion ratio DC-DC converter with low switch voltage stress," *IEEE Trans. Ind. Electron.*, vol. 61, no. 10, pp. 5290–5299, Oct. 2014.

[28] Q. Li *et al.*, "An improved floating interleaved boost converter with the zero-ripple input current for fuel cell applications," *IEEE Trans. Energy Convers.*, vol. 34, no. 4, pp. 2168–2179, Dec. 2019.

[29] N. Rana, M. Kumar, A. Ghosh, and S. Banerjee, "A novel interleaved tri-state boost converter with lower ripple and improved dynamic response," *IEEE Trans. Ind. Electron.*, vol. 65, no. 7, pp. 5456–5465, Jul. 2018.

[30] H. Chen and J. Liao, "Modified interleaved current sensorless control for three-level boost PFC converter with considering voltage imbalance and zero-crossing current distortion," *IEEE Trans. Ind. Electron.*, vol. 62, no. 11, pp. 6896–6904, Nov. 2015.

[31] F. Yu, W. Zhang, Y. Shen, and J. Mao, "A nine-phase permanent magnet electric-drive-reconstructed onboard charger for electric vehicle," *IEEE Trans. Energy Convers.*, vol. 33, no. 4, pp. 2091–2101, Dec. 2018.

[32] X. Wang *et al.*, "Torque ripple reduction in sectored multi three-phase machines based on PWM carrier phase shift," *IEEE Trans. Ind. Electron.*, vol. 67, no. 6, pp. 4315–4325, Jun. 2020.

[33] C. Lin and Y. Tzou, "An innovative multiphase PWM control strategy for a PMSM with segmented stator windings," in *Proc. IEEE Appl. Power Electron. Conf. Expo.*, Mar. 2015, pp. 270–275.

[34] H. Hsu and Y. Tzou, "FPGA control and implementation of a multiphase-interleaved PWM inverter for a segmented PMSM," in *Proc. IEEE 11th Int. Conf. Power Electron. Drive Syst.*, Jun. 2015, pp. 224–230.

[35] J. Wang, Y. Li, and Y. Han, "Evaluation and design for an integrated modular motor drive (IMMD) with GaN devices," in *Proc. IEEE Energy Convers. Congr. and Expo.*, Sep. 2013, pp. 4318–4325.

[36] M. Uğur and O. Keysan, "DC link capacitor optimization for integrated modular motor drives," in *Proc. IEEE 26th Int. Symp. Ind. Electron.*, Jun. 2017, pp. 263–270.

[37] J. Wang, Y. Li, and Y. Han, "Integrated modular motor drive design with GaN power FETs," *IEEE Trans. Ind. Appl.*, vol. 51, no. 4, pp. 3198–3207, Jul. 2015.

[38] L. Verkroost, J. Van Damme, H. Vansompel, F. De Belie, and P. Sergeant, "Module connection topologies and interleaving strategies for integrated modular motor drives," in *Proc. IEEE Int. Electric Mach. Drives Conf.*, May. 2019, pp. 559–564.

[39] D. G. Holmes and T. A. Lipo, *Pulse Width Modulation for Power Converters: Principles and Practice*. Hoboken, NJ, USA: Wiley, 2003.

[40] L. Jin, S. Norrga, O. Wallmark, and N. Apostolopoulos, "Modulation and power losses of a stacked polyphase bridge converter," *IEEE J. Emerg. Sel. Topics Power Electron.*, vol. 5, no. 1, pp. 409–418, Mar. 2017.

[41] B. Rubey, A. Patzak, F. Bachheibl, and D. Gerling, "DC-link current harmonics minimization in ISCAD multi-phase inverters with interleaving," in *Proc. IEEE Vehicle Power Propulsion Conf.*, Dec. 2017, pp. 1–7.

Lynn Verkroost (Student Member, IEEE) was born in Belgium, in 1994. She received the M.Sc. degree in electromechanical engineering from Ghent University, Ghent, Belgium, in 2017, where she is currently working toward the Ph.D. degree in electromechanical engineering.

Since 2017, she has been with the Electrical Energy Laboratory, Department of Electromechanical, Systems and Metal Engineering, Ghent University. Her current research interests include digital, fault tolerant and distributed control of converter-fed electrical machines.

Jordi Van Damme (Student Member, IEEE) was born in Belgium, in 1995. He received the M.Sc. degree in electromechanical engineering from Ghent University, Ghent, Belgium, in 2018, where he is currently working toward the Ph.D. degree in electromechanical engineering.

Since 2018, he has been with the Electrical Energy Laboratory, Ghent University. His current research interests include control of multiphase electrical machines and their condition monitoring.

In 2019, Mr. Van Damme was awarded a Ph.D. fellowship from the Research Foundation-Flanders (FWO).

Dimitar V. Bozalakov (Member, IEEE) was born in Harmanly, Bulgaria, in 1985. He received the M.Sc. degree in industrial electronics from TU Varna, Varna, Bulgaria, in 2011, and the Ph.D. degree in electromechanical engineering from Ghent University, Ghent, Belgium, in 2019.

Since 2019, he is working as a Postdoctoral Assistant with the Electrical Energy Laboratory (EELAB) of Ghent University. His current research interests include electric power systems, renewable energy applications, energy storage, improving the power quality in the distribution grids and efficiency improvement of power electronic converters.

Frederik De Belie (Member, IEEE) was born in Belgium, in 1979. He received the M.Sc. and Ph.D. degrees in electromechanical engineering from Ghent University, Ghent, Belgium, in 2002 and 2010, respectively.

He is currently an Associate Professor with the Department of Electromechanical, Systems and Metal Engineering, Ghent University, where he teaches bachelor's and master's courses in electric drives. His current research interests include identification, monitoring, dynamical modeling and smart control theory applied to power converters and electrical drives.

Dr. De Belie was awarded in 2010 the Iwan Åkerman Award for his Ph.D. work and patent on the seamless integration of sensorless control in drives, awarded on the initiative of Atlas Copco Airpower and Research Foundation Flanders. He is also a member of Flanders Make in the Research Cluster on Control and Decisions.

Peter Sergeant (Senior Member, IEEE)(°1978) received the M.Sc. and Ph.D. degrees in electromechanical engineering from Ghent University, Ghent, Belgium, both in 2001 and 2006.

In 2006, he became a Postdoctoral Researcher with Ghent University (Postdoctoral Fellow of the Research Foundation - Flanders). Since 2012, he has been an Associate Professor with Ghent University. He is also core lab manager in the cluster Motion Products of Flanders Make. His current research domain is electrical machines and drives for industrial and for sustainable energy applications. The focus is on accurate computation of losses in machines and drives, improving energy efficiency and increasing power density.

Hendrik Vansompel was born in Belgium, in 1986. He received the M.Sc, and Ph.D. degrees in electromechanical engineering from Ghent University, Ghent, Belgium, in 2009 and 2013, respectively.

He is currently a Postdoctoral Research Assistant with the Department of Electromechanical, Systems and Metal Engineering, Ghent University. His research interests include electric machines and power electronics.